Materials Research Express

PAPER • **OPEN ACCESS**

Prediction of UHPC mechanical properties using optimized hybrid machine learning model with robust sensitivity and uncertainty analysis

To cite this article: ZhiGuang Zhou *et al* 2025 *Mater. Res. Express* **12** 085703

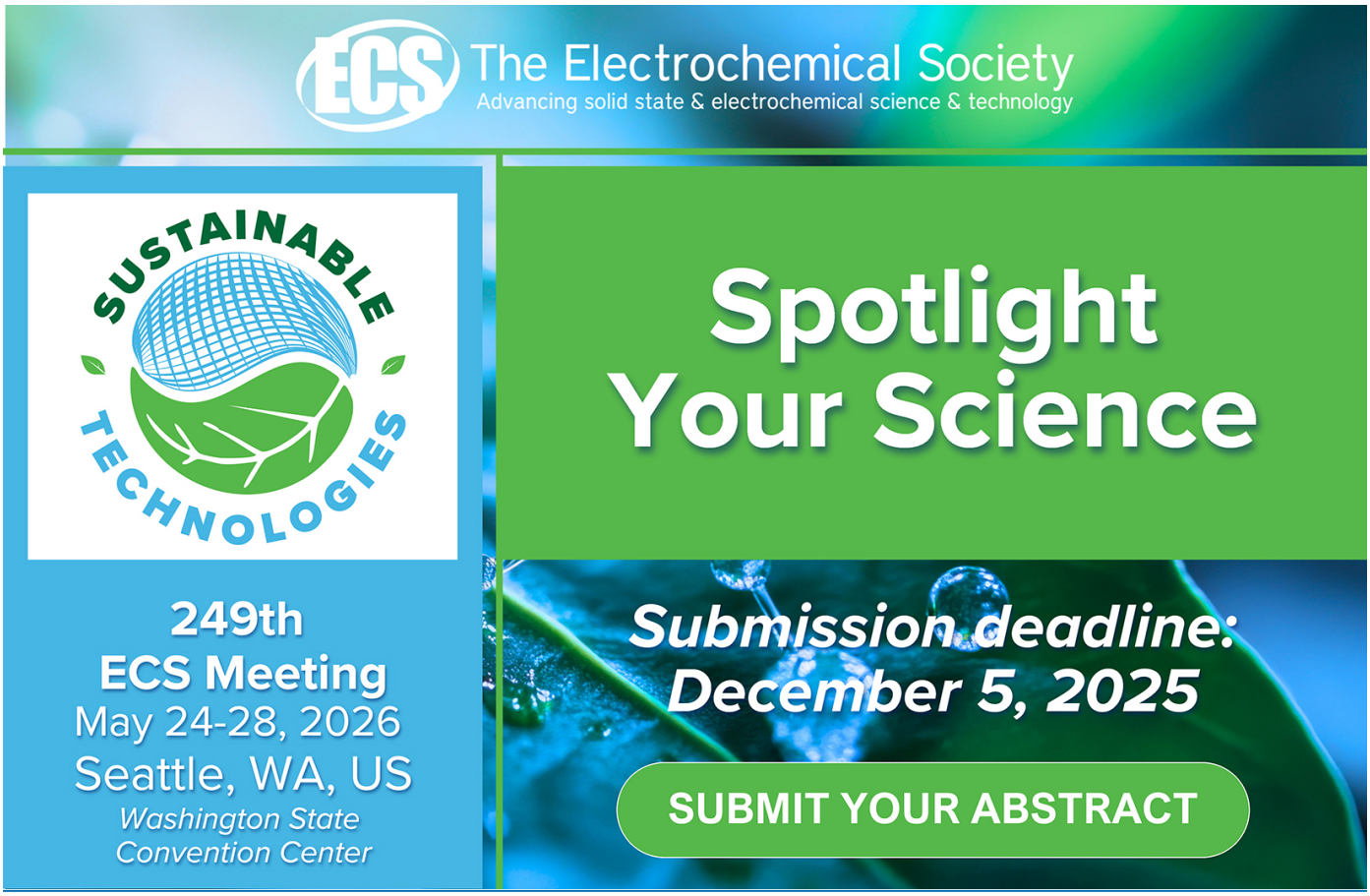

Materials Research Express

PAPER

Prediction of UHPC mechanical properties using optimized hybrid machine learning model with robust sensitivity and uncertainty analysis

ZhiGuang Zhou[1], **Jagaran Chakma**[1,*], **Md Ahatasamul Hoque**[1], **Vaskar Chakma**[2] and **Asif Ahmed**[3]

[1] State Key Laboratory of Disaster Mitigation for Structures, Tongji University, Shanghai, 200092, People's Republic of China
[2] School of Artificial Intelligence and Computer Science, Nantong University, People's Republic of China
[3] Department of Geotechnical Engineering, College of Civil Engineering, Tongji University, Shanghai, 200092, People's Republic of China
[*] Author to whom any correspondence should be addressed.

E-mail: zgzhou@tongji.edu.cn, chakmajagaran@tongji.edu.cn, hoque@tongji.edu.cn, vaskarchakma7@gmail.com and asifahmedbd@tongji.edu.cn

Keywords: UHPC, hybrid machine learning, sensitivity analysis, uncertainty analysis

OPEN ACCESS

RECEIVED
18 June 2025

REVISED
17 July 2025

ACCEPTED FOR PUBLICATION
6 August 2025

PUBLISHED
20 August 2025

Abstract

This study presents a comprehensive evaluation of three hybrid machine learning models XGB-LGB, RF-XGB, and ET-LGB for predicting the mechanical performance of Ultra-High-Performance Concrete (UHPC), including compressive strength (CS), flexural strength (FS), and tensile strength (TS). Each dataset was standardized and split into training (80%) and testing (20%) subsets. Hyperparameter optimization was conducted using a random search algorithm to improve prediction accuracy. The performance of each model was assessed using five key metrics: mean squared error (MSE), root mean squared error (RMSE), mean absolute error (MAE), mean absolute percentage error (MAPE), and coefficient of determination (R^2). This work integrates hybrid ensemble models with SHAP-based explainable AI and uncertainty quantification to achieve high accuracy, model interpretability, and robustness assessment, which are rarely combined in UHPC prediction studies. Among the models, ET-LGB reliably achieved the highest accuracy across all target outputs, with R^2 values reaching 0.99 in both training and testing phases. XGB-LGB also demonstrated strong performance, particularly for CS and FS, achieving R^2 values of 0.99 and 0.98, respectively. In contrast, RF-XGB showed relatively lower accuracy, especially for TS, with R^2 values around 0.93. To improve model interpretability, SHAP-based sensitivity analysis including feature importance plots, beeswarm plots, and heatmaps were employed to analyze the contribution of input features to model predictions. Additionally, an uncertainty analysis was performed to measure the robustness of predictions. Overall, the ET-LGB model proved to be the most reliable and accurate, followed closely by XGB-LGB, demonstrating strong potential for practical UHPC property prediction.

1. Introduction

In recent years, ultra-high-performance concrete (UHPC) has emerged as a groundbreaking cementitious material, garnering much attention for its outstanding mechanical qualities, durability, and sustainability potential [1]. UHPC is defined by a dense matrix formed from optimized combinations of fine aggregates, cement, silica fume, micro-steel fibers, and high-range water-reducing admixtures (HRWR) [2]. It demonstrates compressive strengths surpassing 120 MPa after 28 days of curing, along with exceptional ductility and energy absorption 3 to 16 times greater than conventional concrete and 300 times that of high-performance concrete (HPC) [3]. Its low porosity and high toughness provide exceptional resistance to environmental deterioration, making it suitable for infrastructure subjected to severe circumstances, including maritime settings, seismic zones, and freeze–thaw cycles [4, 5]. In addition to mechanical advantages, UHPC's ability to diminish structural element dimensions—facilitating lighter, thinner, and more aesthetically pleasing designs—establishes it as a

revolutionary solution for contemporary engineering challenges, such as long-span bridges, ultra-high-rise buildings, and resilient infrastructure [6]. Practical applications have been documented across North America, Europe, and Asia, where field projects such as the Mars Hill Bridge (USA), Jakriborg Bridge (Sweden), and Sakata Viaduct (Japan) have demonstrated UHPC's long-term durability and rapid-construction potential under service conditions reported by FHWA and JSCE technical guidelines. Recent improvements have broadened its use, with research investigating the addition of nanomaterials such as graphene oxide to improve fracture resistance and self-healing properties [7]. By reducing material consumption and enhancing durability, UHPC supports global sustainability objectives, providing a means to decrease carbon emissions in construction while maintaining structural integrity. These features jointly emphasize its significance as a fundamental material for promoting building innovation and environmental sustainability [6–9].

Ultra-high-performance concrete (UHPC) is a specialized construction material that incorporates durable fibers, has self-leveling properties, and possesses exceptional strength. It is lightweight and flexible when first combined, but becomes rigid and durable on hardening. Exhibiting flexural, compressive, and tensile strengths of 30 MPa, 150 MPa, and 5 MPa, respectively [10], it surpasses conventional concrete and demonstrates resistance to cracking, corrosion, and severe weather—attributes essential for bridges, skyscrapers, and areas susceptible to earthquakes [11, 12]. Researchers have explored a wide spectrum of steel, basalt, carbon, and polyethylene fibers, revealing that hybrid fiber systems can synergistically enhance post-cracking toughness and strain capacity, while optimized heat-steam curing regimes further accelerate strength gain without compromising durability [13]. However, optimizing UHPC mixtures is complex, since the manufacturing often rely on locally sourced components and need repeated adjustments. Although concrete manufacture accounting for a significant portion of worldwide CO_2 emissions (5%–8%) [13], the enduring lifetime of UHPC substantially decreases emissions over time by significantly lowering the need for repairs and replacements [14]. Innovators are now investigating more sustainable methods, including the replacement of cement with industrial byproducts such as slag or fly ash [15], and the integration of recycled aggregates to minimize environmental impact [16]. Although the initial expenses of UHPC are elevated, its durability, low maintenance requirements, and versatility in addressing contemporary design challenge—such as curved design characteristics or ultra-thin structural elements render it a progressive possibility for sustainable and resilient infrastructure [17].

The advancement of ultra-high-performance concrete (UHPC) relies on an ideal combination of mechanical characteristics, including compressive, flexural, and tensile strength [18], which determine its structural integrity [19]. Conventional mix design, dependent on empirical changes of constituents such as silica fume, steel fibers, and chemical admixtures [20], experiences inherent inefficiencies due to complicated material interactions and extended validation periods. The recent incorporation of machine learning methods, such as ensemble-based machine learning models and optimizing of those models, has enhanced this process by predicting ideal compositions based on previous experimental research, which reduces expensive testing [21, 22]. Complementary meta-heuristic algorithms—genetic algorithms, particle swarm optimization, and ant-colony optimization—have also been coupled with statistical mixture-design frameworks to navigate the high-dimensional UHPC design space more efficiently, pointing toward data-driven, performance-based mix proportioning. These computational methods not only speed up innovation but also promote sustainable practices by minimizing material waste and facilitating environmentally favorable alternatives, in accordance with global decarbonization objectives in construction [9, 23].

Innovative soft computing approaches have emerged as powerful tools for tackling complex issues in engineering, especially in civil engineering, where machine learning (ML) algorithms are transforming material science and design optimization. By using their ability to analysis extensive datasets and determine nonlinear patterns, machine learning models provide accurate predictions of material behaviors, including the mechanical performance of modern concrete composites [24–26]. Methods such as ensemble learning (e.g., gradient boosting, random forest), support vector machines, and deep neural networks have exhibited remarkable flexibility in modelling intricate relationships between mix design parameters and material outcomes, as a result diminishing dependence on expensive research experimentation [3, 27, 28]. Recent studies emphasize its effectiveness in predicting the characteristics of novel materials, such as self-repairing concrete (30), sustainable recycled aggregates, and ultra-high-performance composites [15, 29], highlighting the significance of machine learning in advancing the development of environmentally friendly materials [30]. Furthermore, cross-disciplinary efforts are integrating structural-health-monitoring data streams with ML-based digital twins, enabling real-time performance assessment and proactive maintenance strategies for UHPC infrastructure [31]. These data-driven methodologies not only improve prediction precision but also promote resource efficiency, establishing machine learning as a key component that drives modern civil engineering innovation.

Recent developments in machine learning (ML) have significantly enhanced the predicted accuracy of concrete compressive strength (CS) without requiring substantial laboratory testing. In addition to traditional models like artificial neural networks (ANNs), linear regression, and support vector machines (SVMs),

academics have progressively investigated ensemble learning methods, such as XGBR, CATBoost, Random Forest, Extra tree regressor, and LightGBM which are boosting and bagging algorithms, to improve performance [32, 33]. Research has shown that hybrid models, such LGBM-XGB [31] and SSA-BPNN, SSA-XGB, SSA-SVR, SSA-RFR [34] have enhanced prediction skills by using several machine learning approaches to elucidate complex nonlinear interactions in concrete mixture design. CatBoost was shown to be an excellent model for predicting compressive and tensile strength in fiber-reinforced rubberized recycled aggregate concrete (FRRAC), but Random Forest performed in predicting flexural strength [31]. In parallel, transfer-learning paradigms that reuse pretrained neural-network layers across different concrete datasets have begun to mitigate data-scarcity issues and reduce model-development time, suggesting a promising direction for UHPC applications [35]. Besides, explainable AI methodologies, like SHapley Additive exPlanations (SHAP), have been used to assess the impact of raw material characteristics on CS, hence addressing a significant study deficiency in previous investigations [36]. Future research must concentrate on the integration of physics-informed machine learning models and multi-objective optimization techniques to enhance mixture proportions, facilitating the design of ultra-high-performance concrete (UHPC) with optimized mechanical characteristics and sustainability factors.

Recently, researchers have shown significant interest in hybrid machine learning systems. Numerous studies have shown that the efficacy of individual models such as XGBR, CATBoost, Random Forest, Extra Tree Regressor, and LightGBM in identifying features and quality estimate of extensive datasets pertaining to building materials is undoubtedly substantial [31, 37, 38]. However, prior research on regression analysis of UHPC strength characteristics has only partially explored hybrid model combinations. For instance, a previous study proposed a hybrid XGB-LGB model for predicting compressive and flexural strengths of UHPC using SHAP analysis and grid search optimization. Although their work contributed meaningful insights, it was limited to a single hybrid model and two output properties [37]. Crucially, combining different machine learning models may improve the predictive capability for UHPC strength parameters. In this study, we develop and evaluate three optimized hybrid models to predict compressive, flexural, and tensile strength characteristics of UHPC composites.

This research utilized selected three hybrid machine learning model and optimized them to estimate compressive, flexural, and tensile strength properties of ultra-high-performance concrete, along with high-accuracy algorithms in their applications. Four distinct machine learning model has been selected to build three hybrid distinct models, (XGB and LGB, Random Forest and XGB, Extra tree and LGB) were developed. This study introduces methods that provide superior performance and high predictive accuracy, applicable for predicting the compressive, flexural, and tensile strength of UHPC materials, using input parameters assessed by SHAP interpretation analysis. Hybrid machine learning models performed training, followed by the application of five statistical evaluations during the testing phase: R-squared, root mean square error (RMSE), mean absolute error (MAE), percentage mean absolute error (PMAE), and mean squared error (MSE). The primary objectives of this study were to: (1) establish robust hybrid machine learning model with random search optimization method for improved estimation of the compressive strength (CS), flexural strength (FS), and tensile strength (TS) values of ultra-high-performance concrete (UHPC) matrices, (2) with employing the SHAP interpretation technique for sensitivity analysis to elucidate the opaque nature of predictive estimates and the interrelations among the utilized parameters, and (3) uncertainty analysis of test evaluation results for compressive, flexural, and tensile strength.

2. Methodology

2.1. Dataset preprocessing

Dataset standardization is essential for ensuring the quality and effectiveness of this investigation. In this study, the dataset has standardized by filling zeros with mean data. Given a dataset $\mathbf{X}$ with m rows (samples) and n columns (features), let x_{ij} represent the value of the j -th feature in the i -th sample. If $x_{ij} = 0$, it is replaced by the mean of non-zero values in the j -th column:

$$x'_{ij} = \begin{cases} x_{ij} \ \ if \ \ x_{ij} \neq 0, \\ \mu_j \ \ if \ \ x_{ij} = 0, \end{cases} \tag{1}$$

Where μ_j is the mean of non-zero elements in column j, computed as:

$$\mu_j = \frac{1}{|S_j|} \sum_{i \epsilon S_j} x_{ij}, \ S_j = \{i | \ x_{ij} \neq 0\} \tag{2}$$

Here, S_j is set of row indices where $x_{ij} \neq 0$, and $|S_j|$ is the number of entries column j.

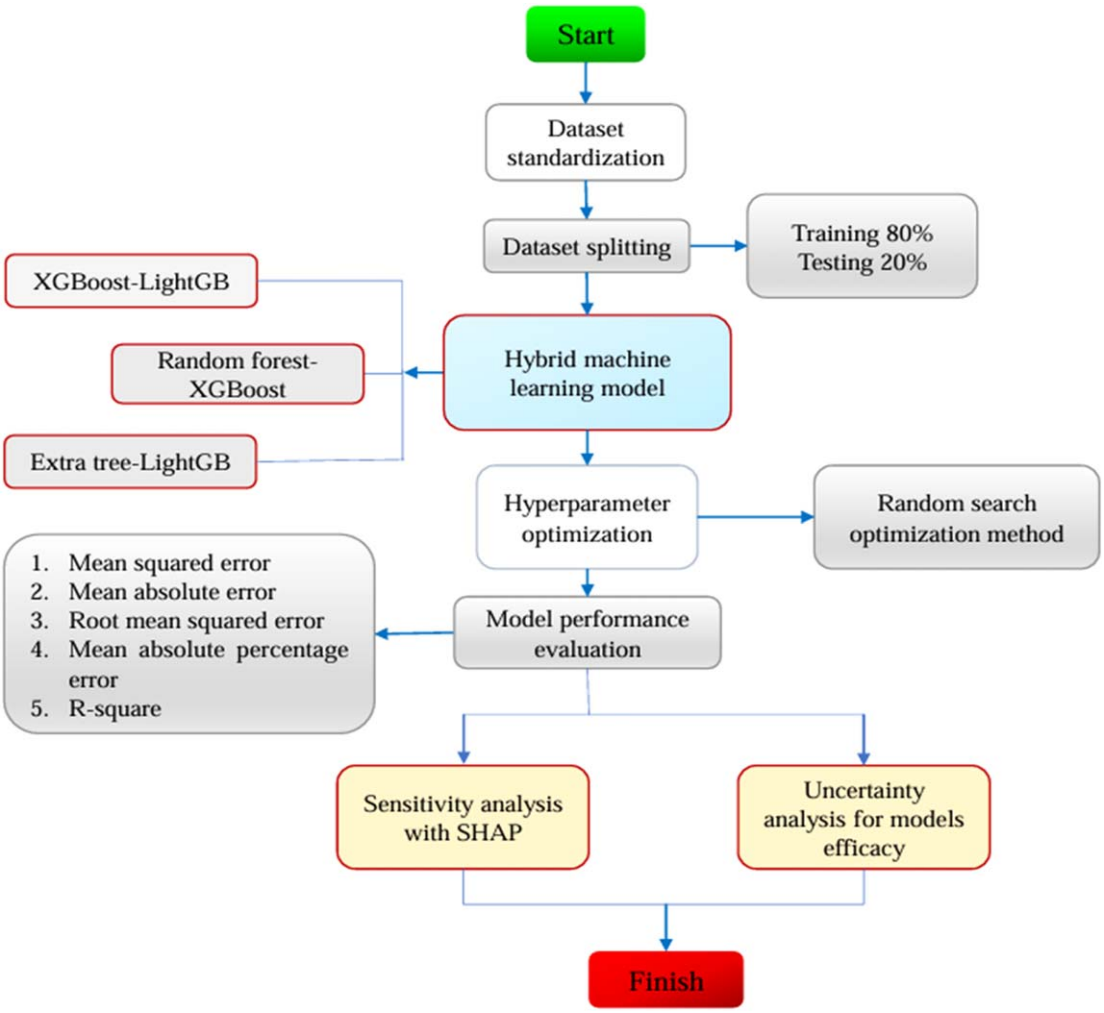

Figure 1. The flowchart of the study for prediction of UHPC properties.

The dataset is randomly divided into training and testing sets, comprising 80% and 20%, respectively. Due to the larger dataset size and still limited availability of test data for UHPC combinations in the literature, the splitting ratio was used. Figure 1 shows the flowchart of the study for prediction of UHPC properties.

2.2. Collected database

This study predicted hybrid machine learning models using literature-based experimental dataset. Previous papers [35, 39–48], provided UHPC mix mechanical property strength values. The number of total data samples for compressive strength is 1041, 311 data samples for flexural strength, and 234 data samples for tensile strength from journal papers were divided into training and testing phases. Training to testing dataset ratio is 8:2. Training AI models to predict output data validity with a certain degree of accuracy is common. Tables 1–3 shows the inputs and outputs data description for compressive, flexural, and tensile strength phases. Input parameters in the data sample greatly affect model performance. The three table presents the fifteen input parameters for three target variables: compressive strength (CS), flexural strength (FS), and tensile strength (TS).

The parameters include cement content, coarse aggregate content, silica fume content, slag powder content, fly ash content, superplasticizer content (SP), sand, water content, high-performance water reducer (HPWR), water-to-binder ratio (w/b), steel fiber content (SF), steel fiber diameter, steel fiber length, hydration temperature (HT), and curing age (Age).

2.3. Correlation analysis of dataset

According to the figures 2–4, the seaborn heatmap approach, which established the impact of interactions between inputs and output parameters, was used to illustrate the correlation [49, 50] coefficient value. The positive and negative effects of the correlation coefficient on input and output characteristics were represented by the various colors. Figure 2 shows, with a value of around 0.40, that age has significant positive impacts on CS properties. Additionally, strength qualities are also impacted by length and SF content. However, certain input

Table 1. Statistical description of compressive strength input and output variables.

Variables	Count	Mean	Std	Min	$P_{25\%}$	$P_{50\%}$	$P_{75\%}$	Max
Cement	1041	975	0	975	975	975	975	975
CA content	1041	933.89	187.83	300	931.29	931.29	1000	1000
Silica fume	1041	170.56	37.86	90	141.04	186.38	186.38	279.2
Slag powder	1041	238.65	71.83	32.5	227.48	227.48	227.48	468.9
Fly ash	1041	175.04	52.96	36	165.10	165.10	165.10	301.76
SP content	1041	26.50	11.71	2.7	25.38	25.38	25.38	88.2
Sand	1041	898.10	180.38	267.85	725	931.75	1062.65	1213
Water	1041	180.58	29.42	132.9	161.5	180	180	293
HPWR	1041	36.18	28.52	0.30	34.76	34.76	35	256
W/B	1041	0.19	0.04	0.12	0.18	0.19	0.21	0.36
SF content	1041	1.95	0.38	0.4	1.91	2	2	4.2
Diameter	1041	204.26	95.28	7	200	200	207.23	500
Length	1041	14.68	4.27	9	13	13	14.47	30
HT	1041	20.59	1.53	20	20	20	20	26
Age	1041	20.06	21.67	1	7	14	28	91
CS	1041	111.15	31.95	12.2	88.4	110.25	130.4	225.5

Table 2. Statistical description of flexural strength input and output variables.

Variables	Count	Mean	Std	Min	$P_{25\%}$	$P_{50\%}$	$P_{75\%}$	Max
Cement	311	803.3	85.24	640	700	850	850	931
CA content	311	964.08	146.40	480	962.89	962.89	962.89	1000
Silica fume	311	185.61	20.61	115	186.71	195.5	195.5	200
Slag powder	311	269.46	64.36	140	267.61	267.61	331.5	331.5
Fly ash	311	132.83	2.89	125	132.83	132.83	132.83	140
SP content	311	15.21	2.73	8	14.68	14.68	14.68	21
Sand	311	856.21	177.52	409	725	935	935	1105
Water	311	171.07	12.91	160	161.5	161.5	180	200
HPWR	311	38.04	6.16	20	35	38.49	42.5	42.5
W/B	311	0.21	0.03	0.16	0.18	0.19	0.19	0.26
SF content	311	2.13	0.51	1	2	2	2	4
Diameter	311	232.31	102.51	20	186	200	218.60	500
Length	311	14.94	4.28	13	13	13	13	25
HT	311	20.53	0.82	20	20	20	20.52	22
Age	311	23.47	18.75	1	7	28	28	90
FS	311	21.67	6.94	7.5	16.83	20.7	25.12	40.8

Table 3. Statistical description of tensile strength input and output variables.

Variables	Count	Mean	Std	Min	$P_{25\%}$	$P_{50\%}$	$P_{75\%}$	Max
Cement	234	810.58	90	640	700	850	850	931
CA content	234	962.89	139.41	480	962.89	962.89	962.89	1000
Silica fume	234	186.71	17.26	115	186.71	186.71	195.5	200
Slag powder	234	267.61	68	140	267.61	267.61	331.5	331.5
Fly ash	234	132.83	2.36	125	132.83	132.83	132.83	140
SP content	234	14.68	0.51	8	14.68	14.68	14.68	21
Sand	234	834.02	161	409	725	840	935	1105
Water	234	170.12	12.70	160	161.5	161.5	180	200
HPWR	234	38.49	5.50	20	35	38.49	42.5	42.5
W/B	234	0.19	0.03	0.16	0.19	0.19	0.19	0.26
SF content	234	2.17	0.58	1	2	2	2	4
Diameter	234	218.60	82.01	20	186	200	200	500
Length	234	14.24	3.43	13	13	13	13	25
HT	234	20.52	0.82	20	20	20	20.52	22
Age	234	24.31	19.97	1	7	28	28	90
TS	234	11.29	4.66	2.8	8.6	11.5	14.3	25.4

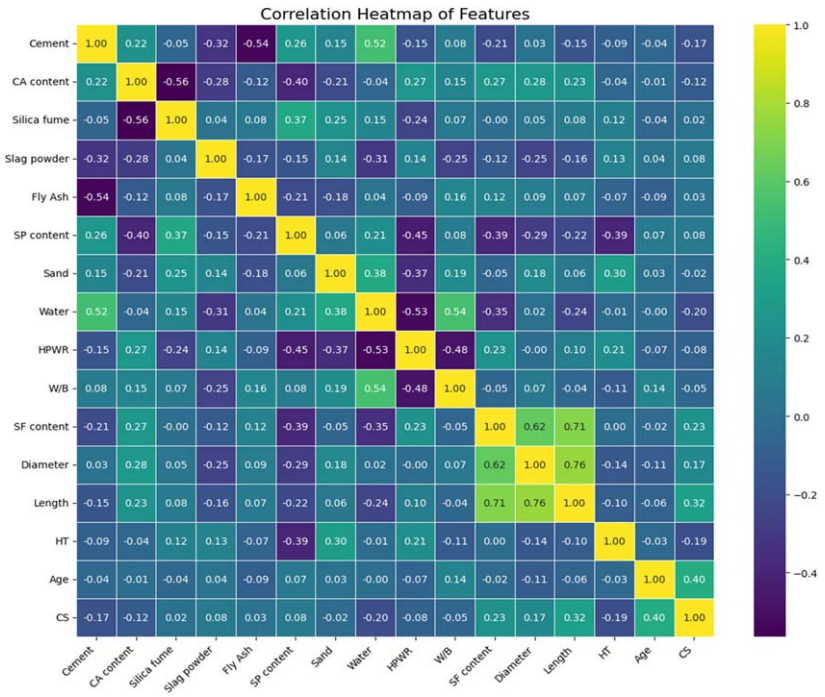

Figure 2. Illustrating Pearson's correlation coefficient of compressive strength.

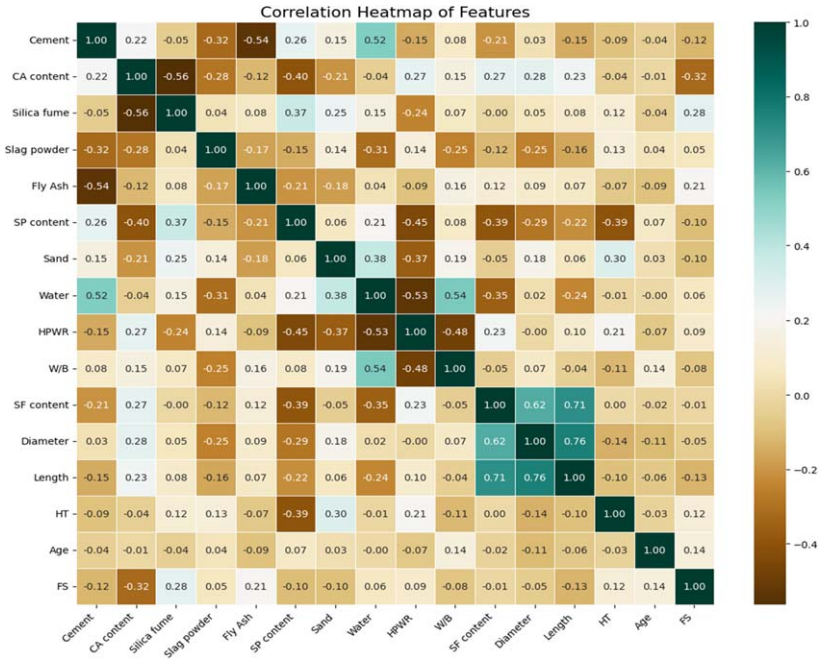

Figure 3. Illustrating Pearson's correlation coefficient of flexural strength.

factors, such water and HT, negatively affect compressive strength. The analytical input parameters for fly ash and silica fume, which have a positive impact on the characteristics of flexural strength, are shown in figure 3 their respective values were 0.28 and 0.21. It is also notable that flexural strength is also influenced by age and HT. But, the flexural strength qualities are negatively impacted by the input parameters of cement, length, and CA content. Figure 4 illustrates the analytical input parameters of slag powder and steel fiber content concentration, which positively affect tensile strength qualities; the values were 0.32 and 0.20, respectively. The diameter, length, and age also affect tensile strength. However, the input parameters of HT, SP content, and CA content negatively influence on the tensile strength qualities.

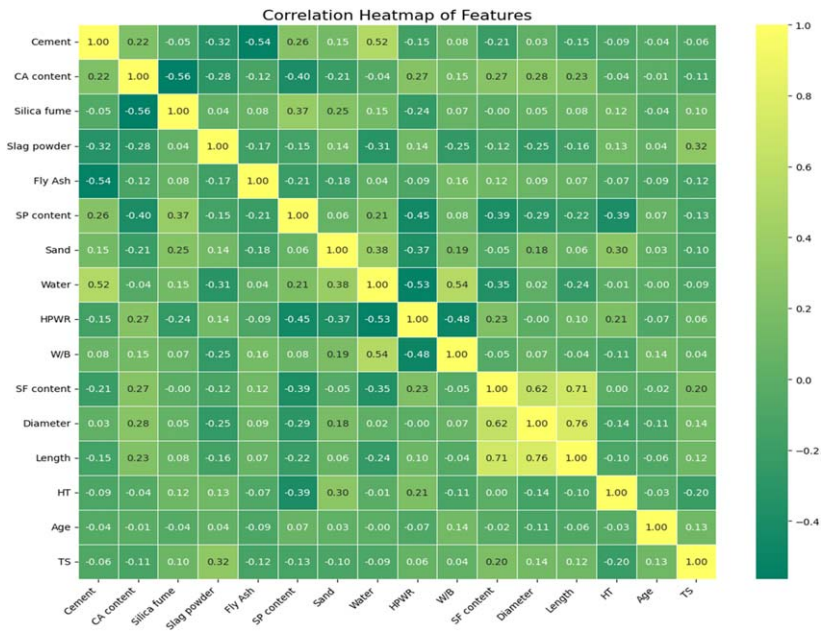

Figure 4. Illustrating Pearson's correlation coefficient of tensile strength.

2.4. Hybrid machine learning models

This study developed three hybrid machine learning models to predict ultra-high-performance concrete characteristics including compressive, flexural, and tensile strength. Each hybrid model combines the predictive capabilities of two ensemble learning algorithms in a two-stage framework, using the first model's result as an input for the second. This strategy maximizes model strengths and minimizes model restrictions to improve prediction framework robustness and generalization. The first hybrid model integrates Extreme Gradient Boosting (XGBoost, known as XGB) with Light Gradient Boosting Machine (LightGBM, known as LGBM). XGB, recognized for its robust regularization and capability to manage intricate nonlinear interactions, is used in the first phase to provide tentative predictions. The predictions are added to the original feature set and sent to the LGBM model in the second step, which is tuned for rapidity and efficiency with large datasets. The second hybrid model utilizes Random Forest (RF) as the initial learner and XGBoost as the subsequent learner. RF, an ensemble approach based on bagging, captures feature interactions and mitigates overfitting by means of the average of many decision trees. The output functions as an enhanced feature for the XGB model, which further improves predictions through boosting mechanism. The third hybrid model combines Extra Trees (ET) with LGBM. ET incorporates enhanced randomization in feature selection and splitting thresholds compared to RF, resulting in enhanced model a range of abilities. Similar to the previous models, ET generates the initial prediction, which is then used by the LGBM model to provide final results.

All hybrid models were trained and verified using the same dataset to ensure consistency and comparability. Hyperparameter tuning was conducted for each learner using a random search with cross-validation to enhance model performance. The predictive outcomes of the three hybrid models were later assessed using usual evaluation metrics, including mean absolute error (MAE) equation (3), mean absolute percentage error (MAPE) equation (4), mean squared error (MSE) equation (5), root mean square error (RMSE) equation (6), and R-squared equation (7) to ascertain the most effective setup for UHPC strength prediction.

$$MAE = \frac{1}{m}\sum_{p=1}^{m}|\hat{y}_p - y_p| \tag{3}$$

$$MAPE = \frac{1}{m}\sum_{p=1}^{m}\frac{|y_p - \hat{y}_p|}{|y_p|} \times 100 \tag{4}$$

$$MSE = \frac{1}{m}\sum_{p=1}^{m}(\hat{y}_p - y_p)^2 \tag{5}$$

$$RMSE = \left(\frac{1}{m}\sum_{p=1}^{m}(y_p - \hat{y}_p)^2\right)^{1/2} \tag{6}$$

$$R^2 = 1 - \frac{\sum_{p=1}^{m}(y_p - \hat{y}_p)^2}{\sum_{p=1}^{m}(y_p - \bar{y})^2} \tag{7}$$

2.5. Hyperparameter optimization

This research used random search optimization to tune the hyperparameters of the hybrid regression models. compared to grid search, random search is more efficient for a substantial number of hyperparameters, since it investigates the search space by sampling a variety of potential with thoroughly assessing each one. This approach enhances the model's predictive accuracy and mitigates the risk of overfitting, particularly when dealing with high-dimensional UHPC data. After tuning, K-fold cross-validation was used to assess the performance of each model with more reliability and to ensure that the findings were not dependent upon a particular train-test split. The tuning and validation procedure were conducted for each hybrid model to determine the optimal set of hyperparameters. Table 4 presents the ideal hyperparameter optimal values achieved by random search for each hybrid model.

2.6. Sensitivity analysis

A sensitivity analysis using SHAP (SHapley Additive exPlanations) values—a cohesive framework based on cooperative game theory—was conducted to measure the extent and direction (positive or negative) of each input feature's impact on the predicted compressive, flexural, and tensile strength values. The SHAP value for a feature denotes the average marginal contribution of that feature over all possible feature combinations. It is computed as:

$$\phi_i = \sum_{S \subseteq F\{i\}} \frac{|S|!(|F| - |S| - 1)!}{|F|!}\left[f(S \bigcup \{i\}) - f(S)\right] \tag{8}$$

Where, ϕ_i is the SHAP value for feature i, F is the set of all input features, S is a subset of F that does not include feature i, $f(S)$ is the model prediction when only the features in S are used, and $|S|$ is the number of features in set S.

To visualize the distribution and impact of these values, SHAP beeswarm plots were used, providing a concise overview of each feature's influence on predictions over all samples. In addition, the feature significance scores obtained from the trained hybrid model were compared with the SHAP-based rankings to verify consistency in the study. In general, these tools provide a coherent and comprehensible insight into model behavior and the significance of each input parameter in UHPC prediction.

2.7. Uncertainty analysis

To assess the robustness of the model predictions, a simple uncertainty index was used, integrating both the precision and variability of the prediction errors. The uncertainty at a 95% confidence level, represented as U, is determined using the following equation:

$$U = z.\sqrt{RMSE^2 + \sigma^2} \tag{9}$$

where, σ is the standard deviation of prediction errors, indicating variability, $RMSE$ measures the average prediction error, $z = 1.96$ corresponds to the 95% confidence level under a normal distribution.

This equation provides a clear and interpretable measure of uncertainty, including both model variability and average error in one result. A reduced U signifies enhanced prediction reliability. This method provides a pragmatic and computationally efficient means to assess uncertainty among various models.

3. Results and discussion

3.1. Predictive performance of hybrid ML models

This section delineates the typical outcomes resulting from the performance measures of the three hybrid models. The models were chosen for each output based on their exceptional performance, shown by low MSE, MAPE, RMSE, and MAE values, as well as high R^2 scores, as seen in figure 11. The regression plots for the XGB-LGB, RF-XGB, and ET-LGB models of each outputs are shown in figures 5–7 respectively.

The hybrid model delineates the relationship between the actual value derived from the experiment and the value generated by the machine learning model. The best line to draw is the one that meets the points where predicts and experimental outcomes align. The model's predictive performance enhances in relation to the distance between the data points and the fitted line. The output generated by each of the three hybrid ml models closely matches predicted values. On reviewing it more closely, the RF-XGB model yields low results compared

Table 4. Hyperparameters optimization for hybrid models.

Hybrid models		Hyperparameter optimization	Optimal values
(1) XGBoost - LightGBM	XGB	Learning rate	0.005
		Reg lembda	10
		Max depth	5
		Min child weight	10
		Gamma	1
		Subsample	0.4
		Colsample bytree	0.4
		No. of estimators	1000
	LGB	Number of leaves	10
		Min sum hessian in leaf	30
		Min split gain	1
		Min data in leaf	50
		Max depth	5
		Max bin	10
		Learning rate	0.03
		Lambda L1	0.1
		Lambda L2	10
		Bagging freq	5
		No. of estimators	200
(2) Random forest - XGBoost	RF	No. of estimators	100
		Max depth	10
		Min samples leaf	300
		Min impurity decrease	0.902
	XGB	No. estimators	10
		Learning rate	0.5
		Max depth	100
		Max bin	1150
		Min child weight	9.301
		Gamma	0.902
		Subsample	0.63
		Reg alpha	0.05
		Reg lambda	0.05
		No. of leaves	100
(3) Extra tree - LightGBM	ET	No. estimators	200
		Max depth	5
		Min samples leaf	1
		Bootstrap	False
		Max features	1.0
	LGB	No. of estimators	9
		Learning rate	0.03
		No. of leaves	150
		Max depth	−1
		Min data in leaf	1
		Feature fraction	1.0

to the other two hybrid models. CS and FS achieved impressive R^2 results in both training and testing sets, with scores of 96 and 94, and 99 and 97, respectively; however, TS is comparatively lower, achieving an R^2 of 93, as seen in figures 6(a)–(c). The XGB-LGB model demonstrates higher performance compared to RF-XGB in both training and testing datasets, with R^2 values for CS, FS, and TS recorded at 99 and 98, 98 and 97, and 95 and 94, respectively, as seen in figures 5(a)–(c). In the ET-LGB model, the actual and predicted values surpass those of the other two models for both training and testing datasets, closely aligning with fit lines of 99 for CS, FS, and TS, as shown in figures 7(a)–(c). These studies demonstrate the capability of three hybrid models to provide precise predictive outputs by correlating input and output characteristics.

Figures 8–10 shows the relative errors, which are defined as the ratio of predicted to actual values, for both the training dataset and the testing dataset. Every single one of the three hybrid models demonstrate outstanding performance, with the majority of relative errors falling inside the proper limits. In terms of CS, the XGB-LGB

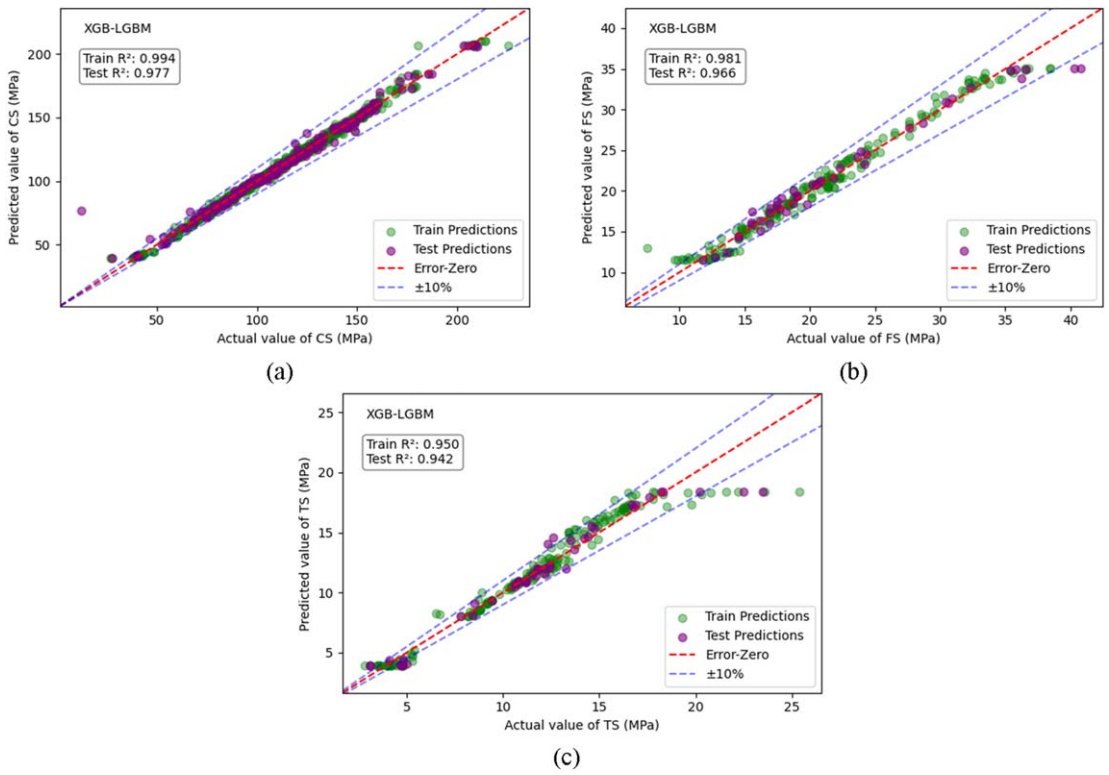

Figure 5. Correlation of actual versus predicted results of (a) CS, (b) FS, and (c) TS obtained from XGB-LGB model.

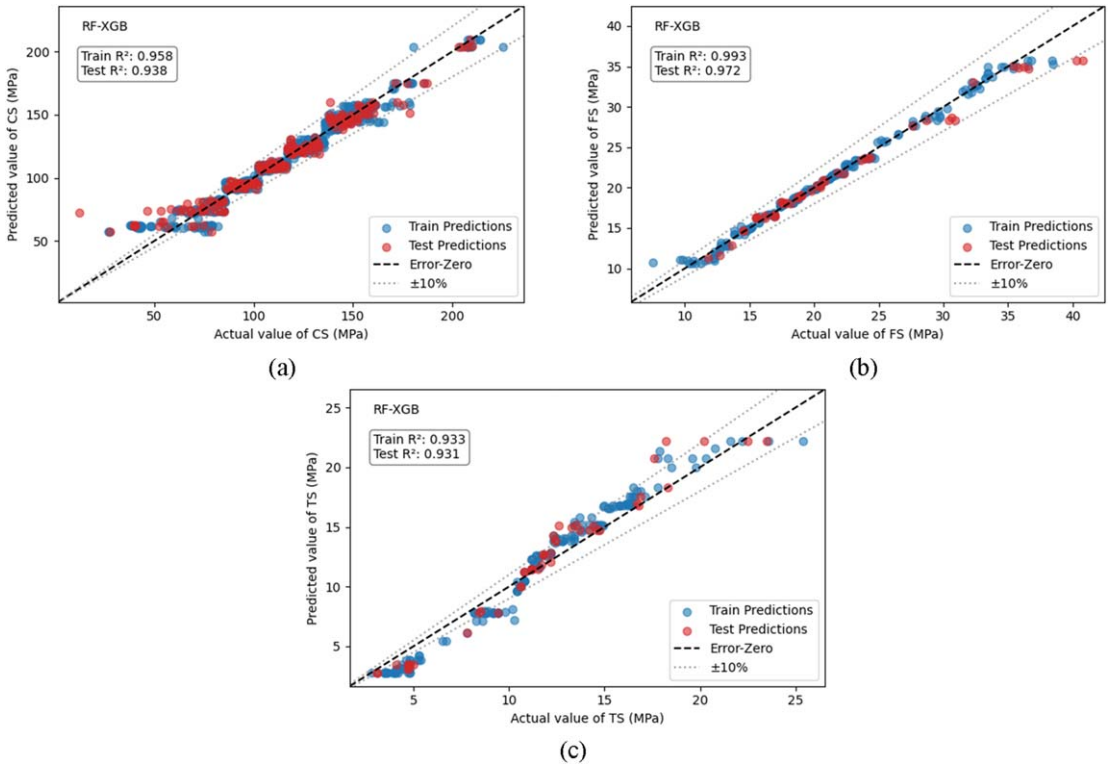

Figure 6. Correlation of actual versus predicted results of (a) CS, (b) FS, and (c) TS obtained from RF-XGB model.

model displays faults that range from +5 to −5, while in terms of FS and TS, errors range from +2 to −2 as shown in figures 8(a)–(c). Although RF-XGB displays slightly higher errors for CS (ranging from +10 to −10), the errors for FS and TS are both contained within the range of +2 to −2 as shown in 9 (a), (b), (c). In general, the

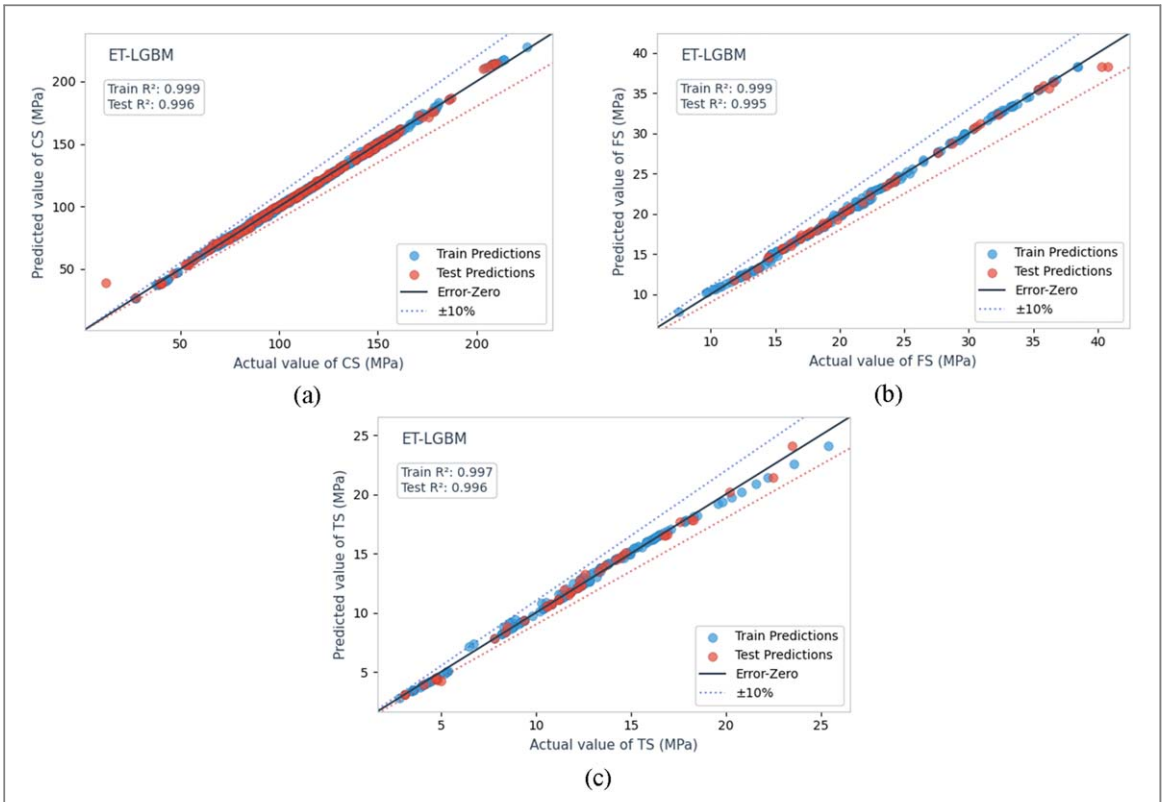

Figure 7. Correlation of actual versus predicted results of (a) CS, (b) FS, and (c) TS obtained from ET-LGB model.

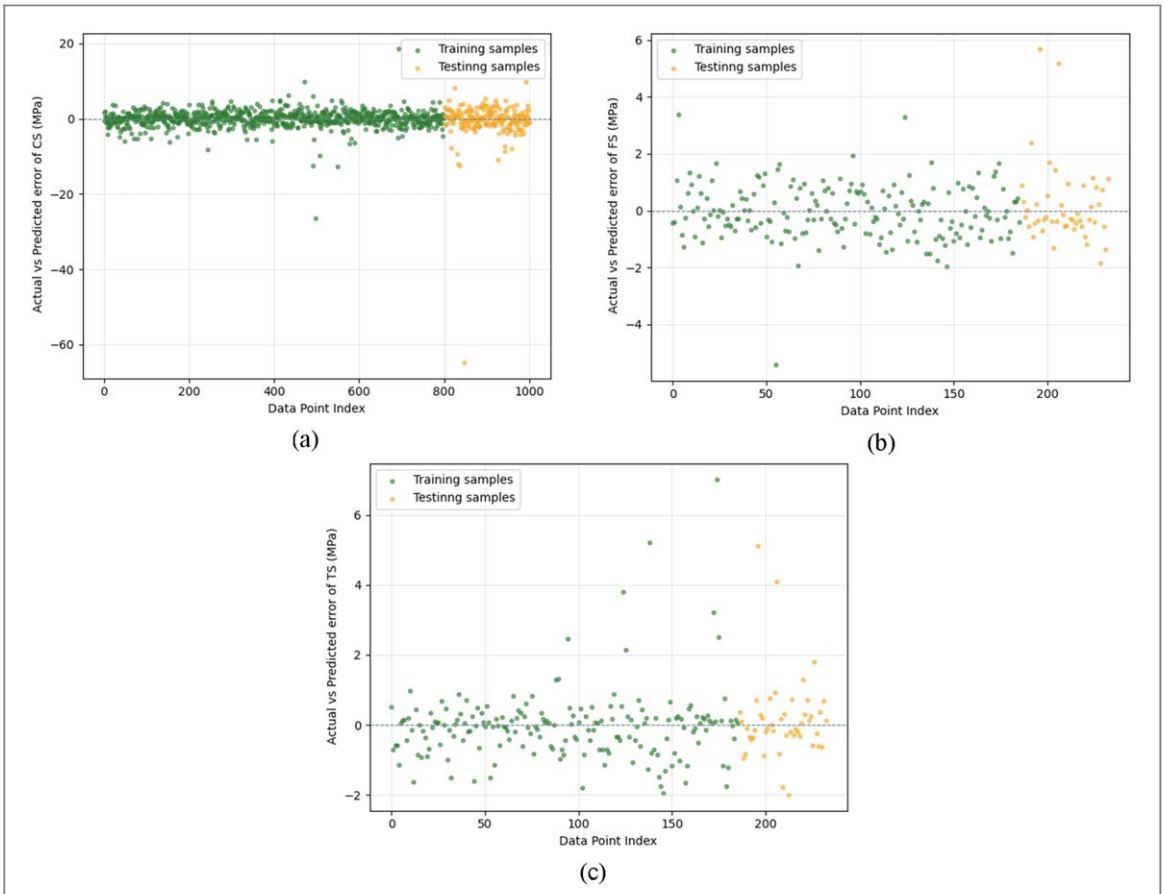

Figure 8. Error prediction of (a) CS, (b) FS, and (c) TS of UHPC obtained from XGB-LGB.

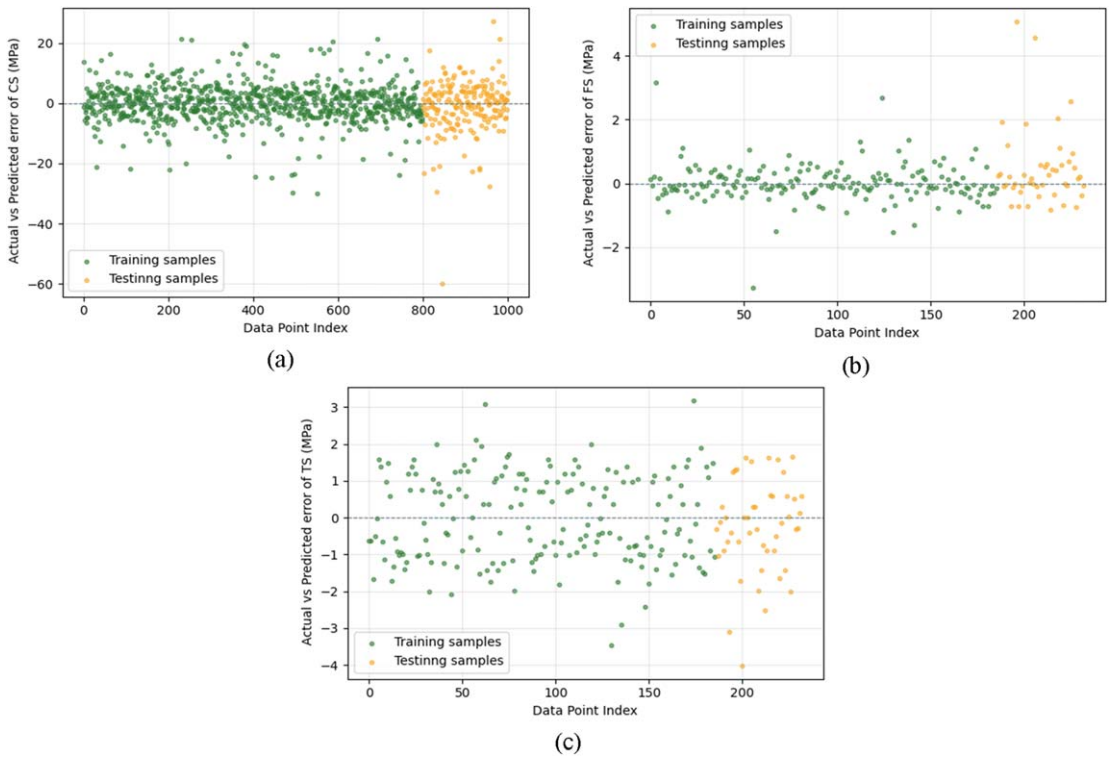

Figure 9. Error prediction of (a) CS, (b) FS, and (c) TS of UHPC obtained from RF-XGB.

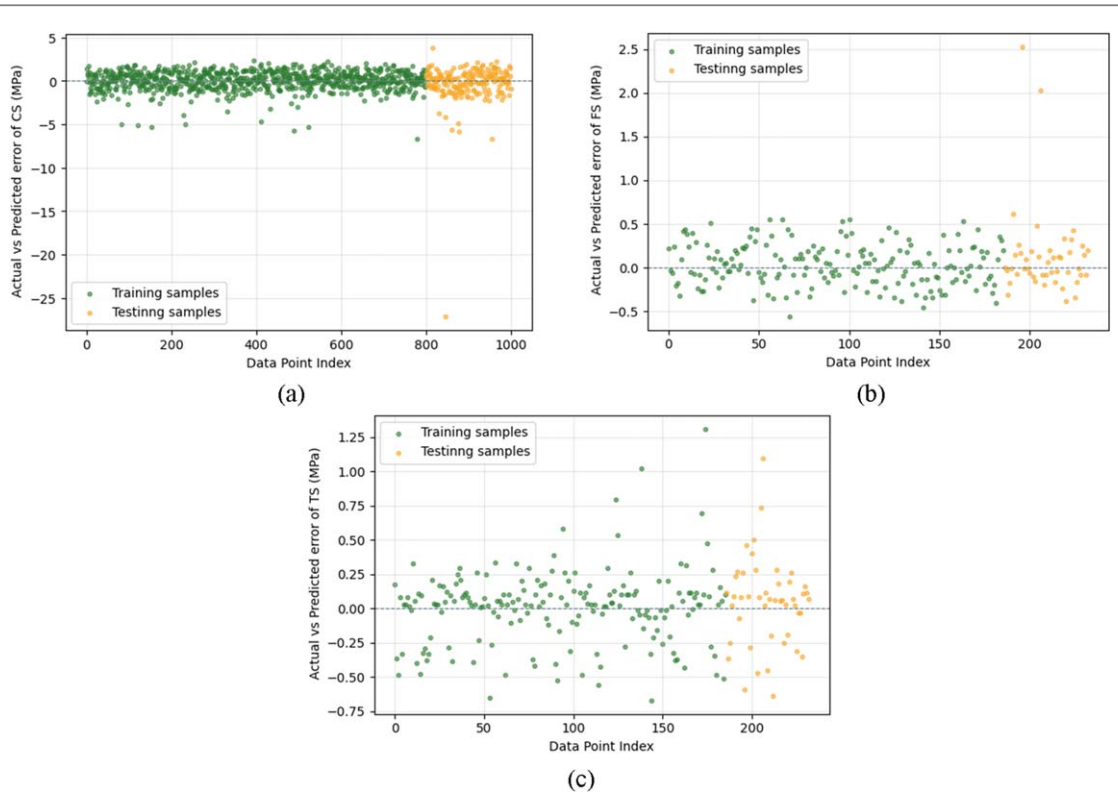

Figure 10. Error prediction of 8(a) CS, 8(b) FS, and 8(c) TS of UHPC obtained from ET-LGB.

ET-LGB model achieves the lowest possible error ranges, which extend from +3 to −3 for CS and only from +0.5 to −0.5 for FS and TS as seen in figures 10(a)–(c). This demonstrates that ET-LGB is capable of producing the most precise and reliable predictions across the board for all outputs.

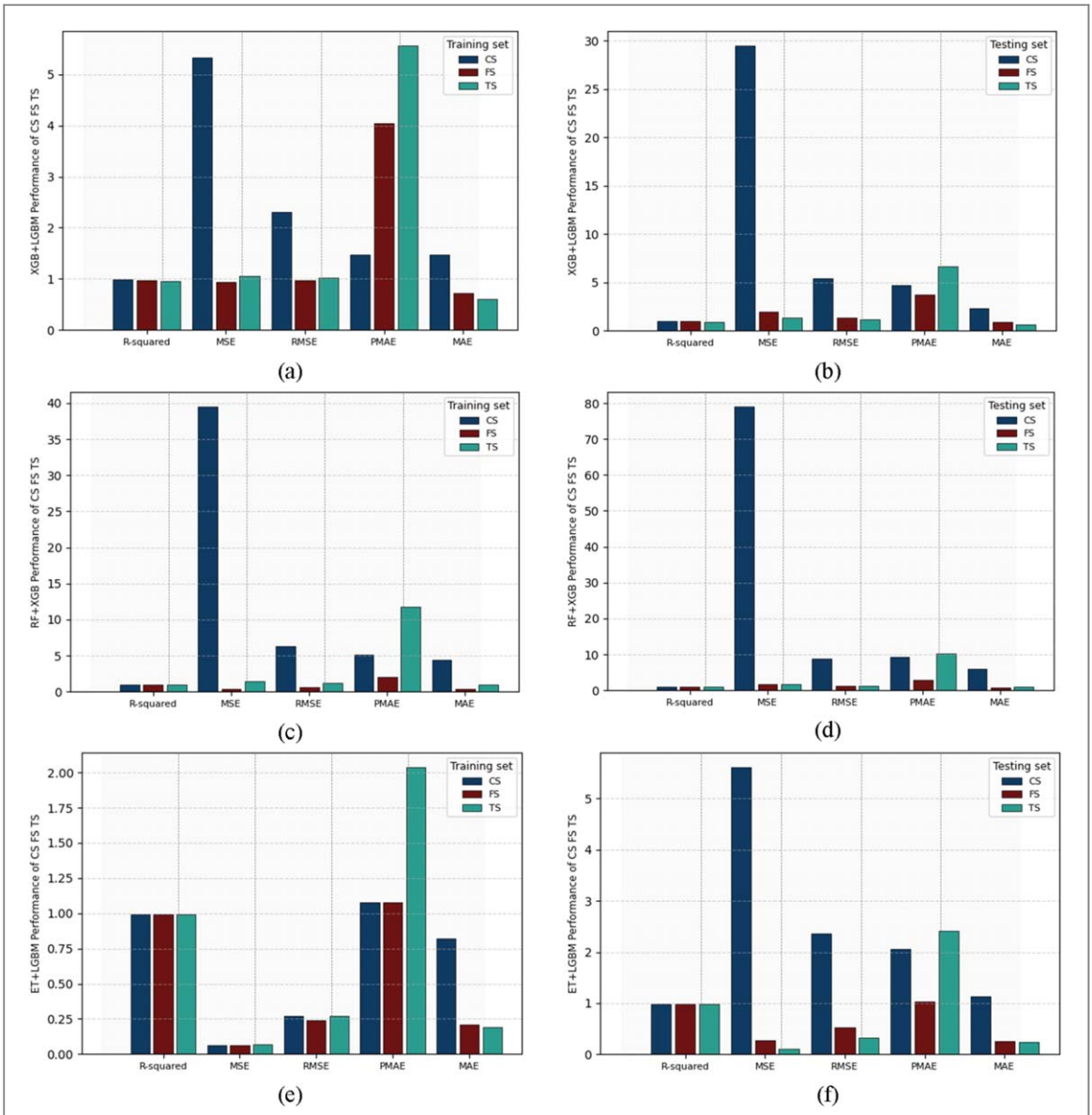

Figure 11. The graphic summary of the model's performance assessment of training and testing sets for CS (a), (b), FS (c), (d), and TS (e), (f) prediction.

3.2. Evaluation of the model's predictive efficacy

This section evaluates the predictive efficacy of the three proposed hybrid models XGB+LGBM, RF+XGB, and ET+LGBM utilizing five principal assessment metrics: R-squared (R^2), Mean Squared Error (MSE), Root Mean Squared Error (RMSE), Mean Absolute Percentage Error (MAPE), and Mean Absolute Error (MAE). Each model underwent training on three distinct datasets (CS, FS, TS), with performance assessed on a common test set to ensure consistency as the results shown in figure 11 and summarizes in table 5.

Models trained on the FS dataset typically attained superior results, shown by the lowest error values and the maximum R^2, signifying robust generalization and predictive precision. The ET+LGBM model trained on FS achieved an MSE of 0.10, RMSE of 0.31, MAE of 0.29, and an R^2 close to 0.99, making it as the most precise and stable model among all tested combinations. The XGB+LGBM model trained on FS showed robust achievement, with MSE and MAE values around 1.0 and an almost perfect R^2. In contrast, models trained on the CS dataset experienced much worse performance, particularly with RF+XGB, where the testing MSE was 79.2, RMSE was 8.9, and MAE exceeded 7.4. The CS-trained model continues to function well, though its accuracy is lower to that of FS and TS. This may be due to the model's lower ability in discerning variations within the dataset. The TS-trained models were excellent results with a low MAE (e.g., 0.28 for ET+LGBM); however, they also exhibited the highest PMAE values, including 5.6 for XGB+LGBM and 2.0 for ET+LGBM, signifying increased percentage errors in relation to actual values. This indicates that while TS-trained models may predict with minimal absolute errors, their predictions may exhibit considerable variation in relative terms, potentially posing challenges in applications that need proportional precision.

Table 5. Evaluation of prediction results on the training and testing sets.

Target values	Hybrid models	Dataset	MSE	MAE	MAPE	RMSE	R^2
Compressive strength	XGB-LGB	Training	5.33	1.47	1.47	2.31	0.99
		Testing	29.52	2.36	4.74	5.43	0.98
	RF-XGB	Training	39.56	4.47	5.13	6.29	0.96
		Testing	79.13	5.88	9.21	8.91	0.94
	ET-LGB	Training	1.21	0.82	0.78	1.11	0.99
		Testing	5.62	1.14	2.06	2.37	0.99
Flexural strength	XGB-LGB	Training	0.94	0.73	4.05	0.97	0.98
		Testing	1.93	0.87	3.74	1.39	0.97
	RF-XGB	Training	0.36	0.38	2.10	0.61	0.99
		Testing	1.61	0.72	2.86	1.26	0.97
	ET-LGB	Training	0.06	0.21	1.08	0.24	0.99
		Testing	0.27	0.26	1.03	0.52	0.99
Tensile strength	XGB-LGB	Training	1.05	0.61	5.57	1.02	0.95
		Testing	1.37	0.68	6.68	1.17	0.94
	RF-XGB	Training	1.41	1.04	11.76	1.19	0.93
		Testing	1.64	0.97	10.33	1.28	0.93
	ET-LGB	Training	0.07	0.19	2.04	0.27	0.99
		Testing	0.10	0.24	2.42	0.32	0.99

In the final analysis, the evaluation demonstrates that training on the FS dataset provides the best results for all models. By obtaining the lowest MSE (0.10), RMSE (0.31), MAE (0.29), and a high R^2 (∼0.99), the ET+LGBM hybrid model stands out among the others. Additionally, it consistently maintains a low PMAE, showing precise and reliable predictions. Overall, ET+LGBM shows the most balanced and reliable performance across all training sets (CS, FS, and TS), often outperforming the other models in key metrics, making it a strong choice for practical applications requiring high accuracy and stability.

3.3. Sensitivity analysis with Shap

A SHapley Additive exPlanations (SHAP) study was performed in order to determine the main input factors affecting the prediction of Ultra-High-Performance Concrete (UHPC) strength characteristics. By measuring the marginal impact of each variable on the model's predictions, the SHAP approach sheds light on both instance-specific contributions and the significance of global features. The best-performing ET-LGB hybrid model in this research is subjected to the SHAP analysis; it continuously surpassed the other model configurations in terms of generalization and predictive accuracy. Below is an analysis of the data for compressive strength (CS), flexural strength (FS), and tensile strength (TS).

The SHAP bar plot in figure 12(a) indicates that curing age is the predominant variable influencing compressive strength, with a mean SHAP value of 18.25. This significant effect indicates the continuous hydration process and microstructural evolution throughout time. The subsequent critical factors are diameter (7.93) and water-to-binder ratio (W/B)* (7.63), both of which substantially influence the mixture's porosity and load-distribution capacity. Cement, sand, and steel fiber content are relatively influential characteristics, but slag powder, silica fume, and superplasticizer content have a more restricted effect. The SHAP beeswarm plot in figure 13(a) indicates that higher age and diameter values favorably influence CS, but high W/B ratios adversely affect the outcome. Silica fume, slag powder, and SF concentration have inconsistent but localized effects. The distribution of SHAP values validates the non-linear and instance-specific impacts of these factors. The SHAP heatmap in figure 14(a) offers sample-specific insights, highlighting substantial and persistent influences from age, diameter, and W/B. The red color gradients for these characteristics in high-output examples indicate their beneficial impact. Inferior-ranked variables exhibit mostly muted or neutral patterns, signifying minimal or insignificant contributions.

The SHAP importance plot in figure 12(b) indicates that the high-performance water reducer (HPWR) is the primary contributing variable to flexural strength, with a SHAP value of 3.11, highlighting its significance in enhancing flowability and matrix uniformity. In the meantime, age (1.91), SF amount (1.37), and cement (1.17) are identified as factors that affect fiber dispersion and matrix reinforcement. The beeswarm plot in figure 13(b) confirms these results, indicating that higher amounts of HPWR, age, and SF content positively influence FS predictions. SP content and W/B have little influence. The distribution of SHAP values indicates that these primary factors consistently influence the majority of samples. The heatmap in figure 14(b) supports this, displaying prominent red bands for HPWR, age, and SF content in high-output predictions. Additional inputs

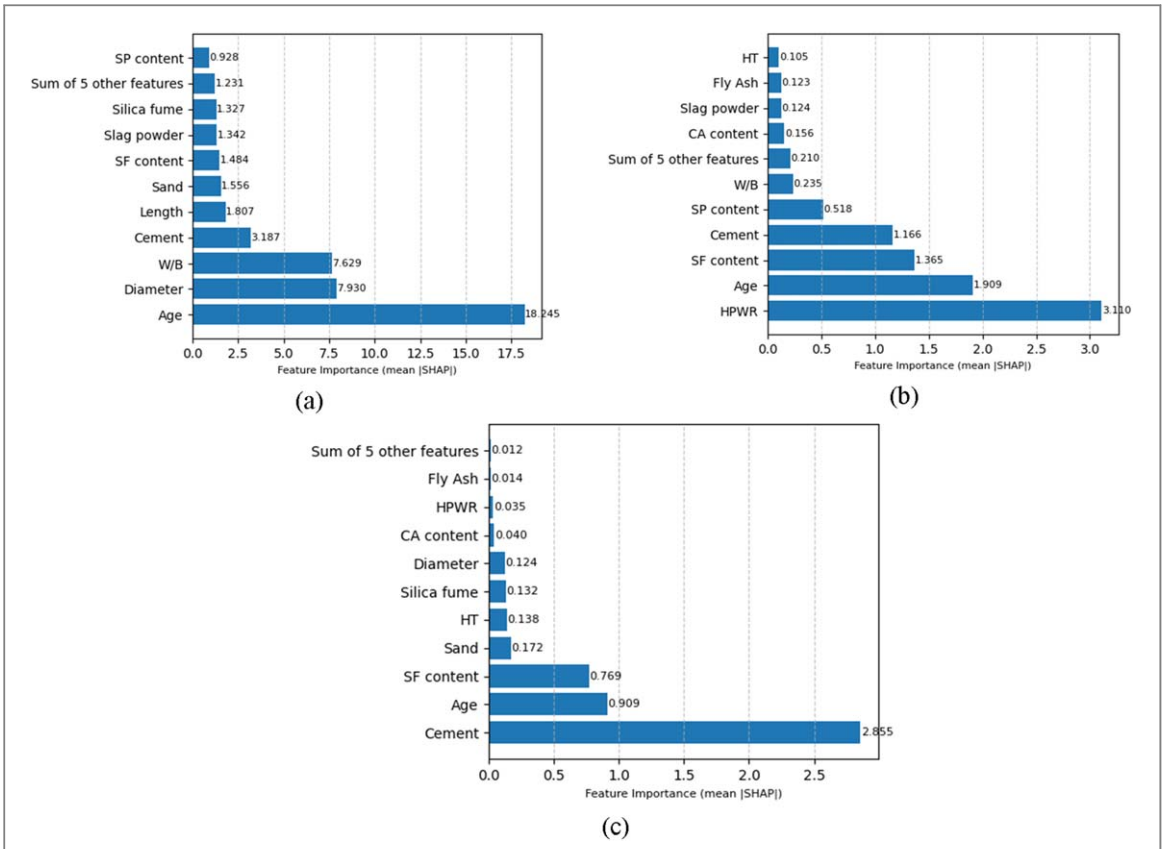

Figure 12. Features importance factor of ET-LGB for CS (a), FS (b), and TS (c).

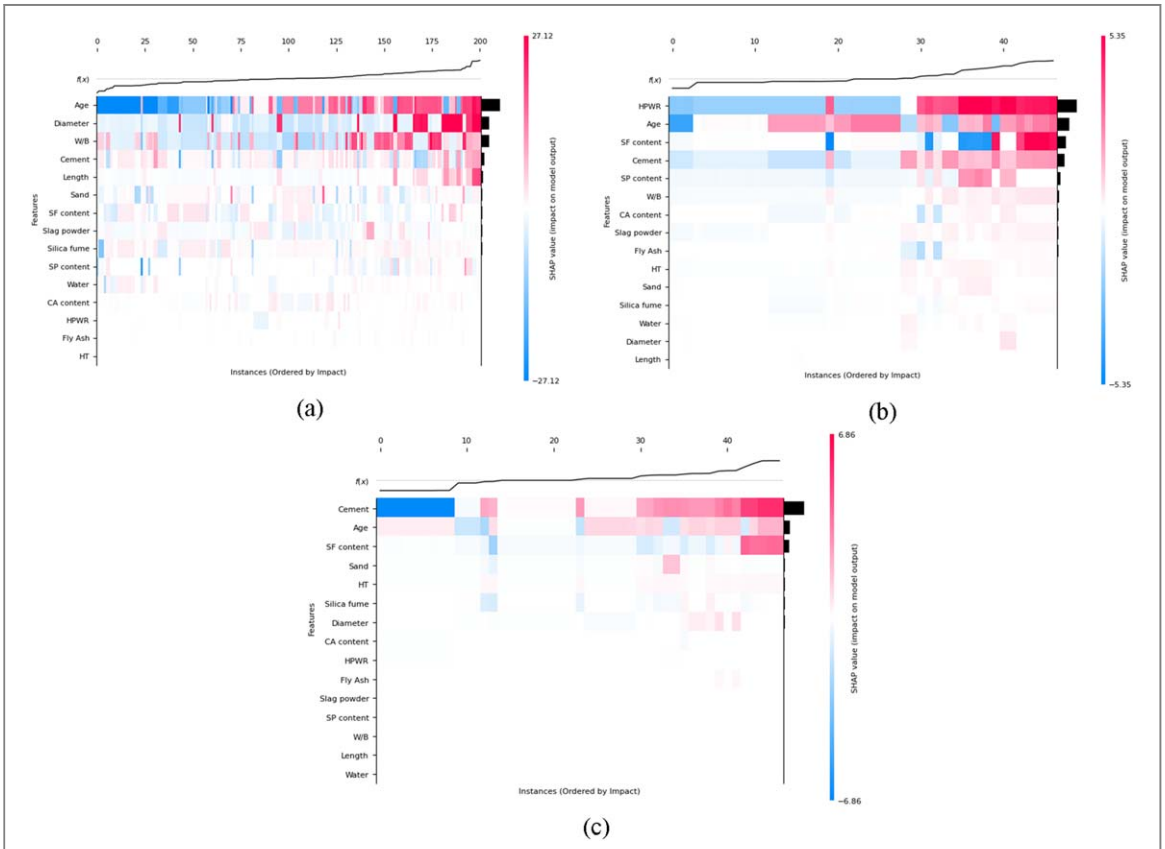

Figure 13. Beeswarm plots of features of ET-LGB for CS (a), FS (b), and TS (c).

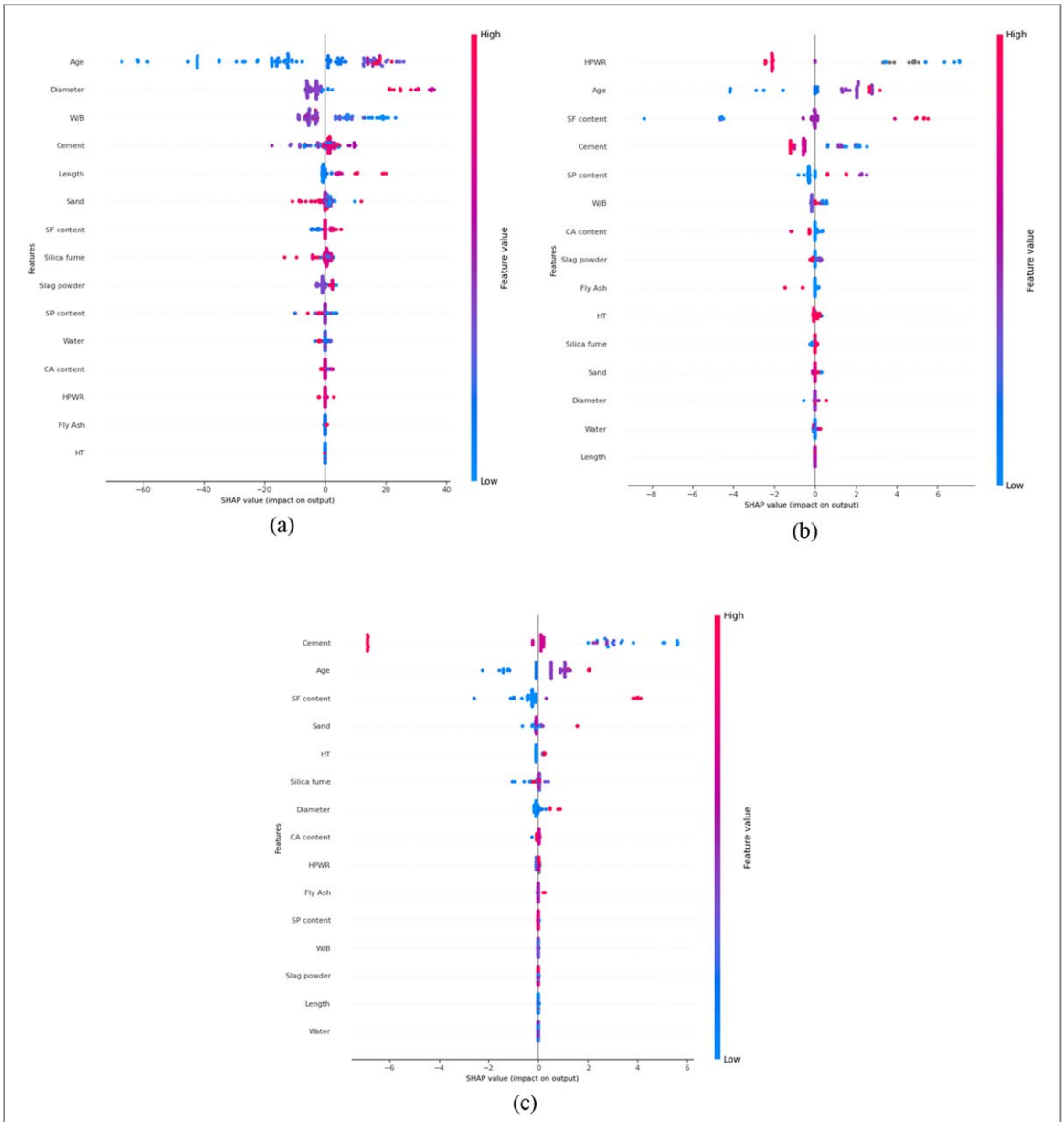

Figure 14. SHAP impact values on outputs of ET-LGB for CS (a), FS (b), and TS (c).

such fly ash, sand, and silica fume demonstrate diminished and variable SHAP magnitudes, underscoring their restricted independent impact on FS prediction.

The SHAP relevance plot in figure 12(c) for predicting tensile strength indicates that cement is the most significant factor (SHAP value: 2.86), next to age (0.91) and SF content (0.77). These findings correspond with the anticipated performance of matrix-dense materials and fiber reinforcement in tensile applications. The beeswarm plot in figure 13(c) illustrates that higher levels of cement and age are associated with significant positive SHAP impacts, but other features—such as HPWR, SP content, and fly ash—exhibit negligible contributions, shown by their SHAP values clustering at zero. The SHAP heatmap in figure 14(c) illustrates that the most influential factors (cement, age, and, to a lesser degree, SF content) are shown in red coloring for high-strength occurrences, emphasizing their significant positive contributions. The residual input characteristics have dispersed or feeble color intensity, signifying little impact on the TS prediction.

The SHAP analysis using the ET-LGB hybrid model demonstrates property-specific feature sensitivity in UHPC strength predictions: The curing age is the key factor for all three parameters, particularly for compressive strength and flexural strength. Cement has the most significant impact on TS, with minor impacts on CS and FS. HPWR has significant influence on FS, but not in TS or CS. The presence of SF content enhances both FS and TS, indicating its contribution to the enhancement of flexibility and fiber-matrix interaction. Characteristics such as water-to-binder ratio and diameter are more crucial to compressive strength, while factors like fly ash, high-temperature materials, and superplasticizer concentration have less overall influence.

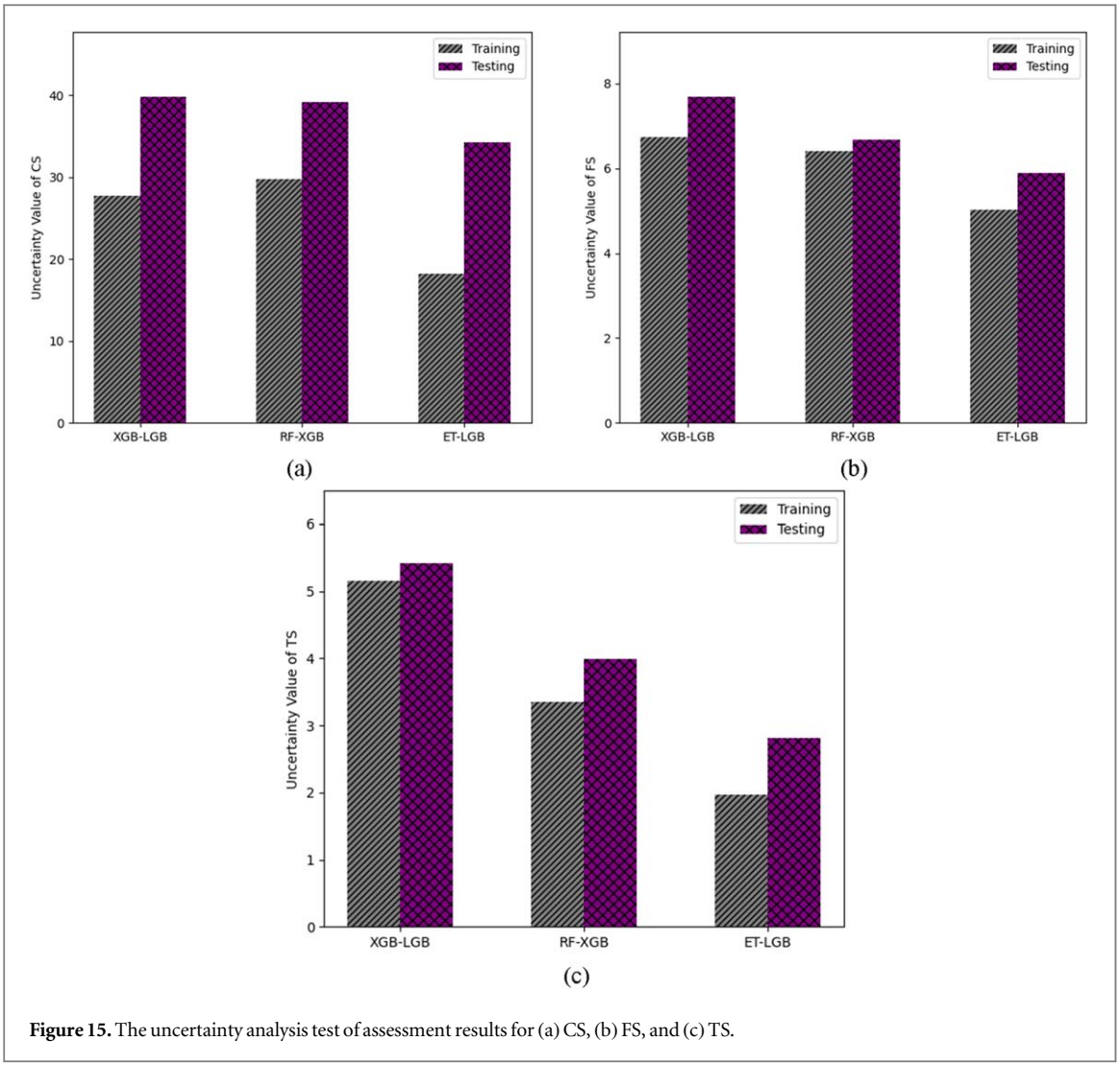

Figure 15. The uncertainty analysis test of assessment results for (a) CS, (b) FS, and (c) TS.

This research integrates SHAP bar plots, beeswarm plots, and heatmaps to provide a thorough comprehension of feature effect on both global and local scales. These findings not only confirm the precision of the ET-LGB model but also provide practical insights for enhancing UHPC mix designs to achieve particular mechanical performance objectives.

3.4. Analysis of uncertainty

Figure 15 presents the results of the uncertainty analysis for CS, FS, and TS during both the training and testing phases. Figure 15(a) illustrates that the ET-LGB model achieves the lowest uncertainty for CS throughout both training and testing phases, signifying robust predictive reliability and generalization. On the other hand, the RF-XGB model has highest uncertainty during both phases, indicating less consistency in its predictions. In figure 15(b), the ET-LGB model demonstrates the lowest uncertainty for FS in both stages. The RF-XGB model has moderate uncertainty, but the XGB-LGB model displays the greatest uncertainty, indicating less stability for this output. In figure 15(c), the ET-LGB model consistently outperforms the other models by achieving the minimal uncertainty for TS in both training and testing stages. The RF-XGB model has modest performance, but the XGB-LGB model yields the largest uncertainty values.

Overall, the ET-LGB hybrid model consistently provides the most stable and reliable predictions for all three mechanical properties, confirming its exceptional capability to mitigate uncertainty in UHPC property estimate.

4. Conclusion

This study predicted the compressive, flexural, and tensile strength characteristics of UHPC materials using three hybrid machine learning models: XGB-LGB, RF-XGB, and ET-LGB. The hyper-parameters of these hybrid machine learning models are well-aligned to provide high-accuracy predictions for the compressive,

flexural, and tensile strength of ultra-high-performance concrete (UHPC). The compiled database was normalized by imputing missing values with the mean and thereafter divided into training (80%) and testing (20%) sets. Additionally, the assessment of the precision of all models use quality of fit parameters. The SHAP algorithm analysis was used to assess the positive and negative impacts of input factors on the output compressive, flexural, and tensile strength. Finally, uncertainty analysis has been conducted for the performance of the hybrid models.

1. A heatmap of the correlation coefficient showed input-output interactions. The age input factors strongly impact compressive strength characteristics, with a correlation value of 0.40. The analytical input parameters of silica fume and fly ash improve flexural strength by 0.28 and 0.21, accordingly. Additionally, the tensile strength is positively influenced by slag powder and steel fiber content, with values of 0.32 and 0.20, respectively.
2. The hybrid ET-LGB model demonstrated high predictive efficiency for compressive, flexural, and tensile strength with an error range of 5 MPa for compressive strength and 0.5 for flexural and tensile strengths throughout training and testing phases. Over 99% of hybrid ET-LGB model data points matched with the linear 1:1 line. The three Hybrid ML models' error proportions dropped to a reasonable range of $\pm$ 10%.
3. The research evaluates model performance using five statistical metrics. The ET-LGB model for compressive, flexural, and tensile strength achieved the highest R-squared values, 0.99, throughout training and testing. XGB-LGB and RF-XGB both showed high R-square values, with CS obtaining 0.99 and 0.97 and 0.96 and 0.94 during training and testing. FS scores 0.98 and 0.97 for XGB-LGB and 0.99 and 0.97 for RF-XGB across both phases. TS scores for the XGB-LGB model are 0.95 and 0.94, whereas the RF-XGB model is 0.93 in both sets. RMSE value from hybrid ET-LGB model is significant. The hybrid ML model's R-square value indicated outstanding performance across all output parameters, with the hybrid ET-LGB model topping the other two hybrid models.
4. The Shapley Additive Explanations analysis from the hybrid ET-LGB model indicated that curing age, HPWR, and cement content are the main variables influencing the enhancement of compressive strength (CS), flexural strength (FS), and tensile strength (TS) of UHPC materials. The compressive, flexural, and tensile strength output factors strongly correlate with the increase in steel fiber diameter and the age parameters of UHPC. Although improved results are seen for low values of HT, steel fiber length, and the water parameters CS, FS, and TS.

Acknowledgments

The authors wish to gratefully acknowledge the support of this work by the National Key Research and Development Program of China under Grant No. 2024YFC3015100.

Data availability statement

The data cannot be made publicly available upon publication because they are owned by a third party and the terms of use prevent public distribution. The data that support the findings of this study are available upon reasonable request from the authors.

CRediT authorship contribution statement

ZhiGuang Zhou: Supervision, Investigation, Conceptualization, Methodology, Writing–original draft. **Chakma Jagaran:** Data curation, Methodology, Data generation, Validation, Writing–original draft, Investigation. **Md Ahatasamul Hoque:** Data generation, Writing—review & editing, Investigation, Supervision. **Vaskar Chakma:** Methodology, Writing—review & editing, Validation, Data curation, Visualization. **Asif Ahmed:** Writing—review & editing, Investigation.

Declaration of competing interest

The authors declare that they have no known competing financial interests or personal relationships that could have appeared to influence the work reported in this paper.

Author contributions

ZhiGuang Zhou 0000-0002-2799-0724
Conceptualization (equal), Investigation (equal), Methodology (equal), Supervision (equal), Writing – original draft (equal)

Jagaran Chakma 0009-0001-1688-8097
Data curation (equal), Investigation (equal), Methodology (equal), Validation (equal), Writing – original draft (equal)

Md Ahatasamul Hoque
Data curation (equal), Investigation (equal), Supervision (equal), Writing – review & editing (equal)

Vaskar Chakma 0009-0003-3039-3175
Data curation (equal), Methodology (equal), Validation (equal), Visualization (equal), Writing – review & editing (equal)

Asif Ahmed
Investigation (equal), Writing – review & editing (equal)

References

[1] Li J, Wu Z, Shi C, Yuan Q and Zhang Z 2020 Durability of ultra-high performance concrete—a review *Constr. Build. Mater.* **255** 119296
[2] Ullah R, Qiang Y, Ahmad J, Vatin N I and El-Shorbagy M A 2022 Ultra-high-performance concrete (UHPC): a state-of-the-art review *Materials* **15** 4131
[3] Marani A, Jamali A and Nehdi M L 2020 Predicting ultra-high-performance concrete compressive strength using tabular generative adversarial networks *Materials* **13** 4757
[4] Nilimaa J 2023 Smart materials and technologies for sustainable concrete construction *Developments in the Built Environment* **15** 100177
[5] Saeed F H and Hejazi F 2025 A comprehensive review of retrofitted reinforced concrete members utilizing ultra-high-performance fiber-reinforced concrete *Materials* **18** 945
[6] Shen Z, Deifalla A F, Kamiński P and Dyczko A 2022 Compressive strength evaluation of ultra-high-strength concrete by machine learning *Materials* **15** 3523
[7] Khalid M Y, Kamal A, Otabil A, Mamoun O and Liao K 2023 Graphene/epoxy nanocomposites for improved fracture toughness: a focused review on toughening mechanism *Chemical Engineering Journal Advances* **16** 100537
[8] Kim H, Koh T and Pyo S 2016 Enhancing flowability and sustainability of ultra high performance concrete incorporating high replacement levels of industrial slags *Constr. Build. Mater.* **123** 153–60
[9] Althoey F, Ansari W S, Sufian M and Deifalla A F 2023 Advancements in low-carbon concrete as a construction material for the sustainable built environment *Developments in the Built Environment* **16** 100284
[10] Zhang R, Hu P, Chen K, Li X and Yang X 2021 Flexural behavior of T-shaped UHPC beams with varying longitudinal reinforcement ratios *Materials* **14** 5706
[11] Akhnoukh A K and Buckhalter C 2021 Ultra-high-performance concrete: constituents, mechanical properties, applications and current challenges *Case Studies in Construction Materials* **15** e00559
[12] Firoozi A A, Firoozi A A, Oyejobi D O, Avudaiappan S and Flores E S 2024 Emerging trends in sustainable building materials: Technological innovations, enhanced performance, and future directions *Results in Engineering* **24** 103521
[13] Kirthiga R and Elavenil S 2024 A survey on crack detection in concrete surface using image processing and machine learning *J. Build Rehabil [Internet]* [cited 2025 Jul 15] **9** Available from: https://link.springer.com/10.1007/s41024-023-00371-6
[14] Khaiyum M Z, Sarker S and Kabir G 2023 Evaluation of carbon emission factors in the cement industry: an emerging economy context *Sustainability* **15** 15407
[15] Abellán-García J, Carvajal-Muñoz J S and Ramírez-Munévar C 2024 Application of ultra-high-performance concrete as bridge pavement overlays: literature review and case studies *Constr. Build. Mater.* **410** 134221
[16] Perera M A G P and Ranjith P 2024 Eco-friendly cementitious composites for enhanced strength: emerging trends and innovations *J. Clean. Prod.* **468** 142962
[17] Neupane R P, Devi N R, Imjai T, Rajput A and Noguchi T 2025 Cutting-edge techniques and environmental insights in recycled concrete aggregate production: a comprehensive review *Resources, Conservation & Recycling Advances* **25** 200241
[18] Kravanja G, Mumtaz A R and Kravanja S 2024 A comprehensive review of the advances, manufacturing, properties, innovations, environmental impact and applications of ultra-high-performance concrete (UHPC) *Buildings* **14** 382
[19] Meng W and Khayat K H 2016 Mechanical properties of ultra-high-performance concrete enhanced with graphite nanoplatelets and carbon nanofibers *Composites* B **107** 113–22
[20] Bahmani H, Mostafaei H, Santos P and Fallah Chamasemani N 2024 Enhancing the mechanical properties of ultra-high-performance concrete (UHPC) through silica sand replacement with steel slag *Buildings* **14** 3520
[21] Mastali M and Dalvand A 2016 Use of silica fume and recycled steel fibers in self-compacting concrete (SCC) *Constr. Build. Mater.* **125** 196–209
[22] Wakjira T G, Kutty A A and Alam M S 2024 A novel framework for developing environmentally sustainable and cost-effective ultra-high-performance concrete (UHPC) using advanced machine learning and multi-objective optimization techniques *Constr. Build. Mater.* **416** 135114
[23] Sun C, Wang K, Liu Q, Wang P and Pan F 2023 Machine-learning-based comprehensive properties prediction and mixture design optimization of ultra-high-performance concrete *Sustainability* **15** 15338

[24] Li Y et al 2024 Artificial intelligence in net-zero carbon emissions for sustainable building projects: a systematic literature and science mapping review Buildings 14 2752
[25] Nunez I et al 2021 Estimating compressive strength of modern concrete mixtures using computational intelligence: a systematic review Constr. Build. Mater. 310 125279
[26] Okasha N M et al 2024 Machine learning approach to predict the mechanical properties of cementitious materials containing carbon nanotubes Developments in the Built Environment 19 100494
[27] Kibrete F, Trzepieciński T, Gebremedhen H S and Woldemichael D E 2023 Artificial intelligence in predicting mechanical properties of composite materials Journal of Composites Science 7 364
[28] Hao J, Jiao W, Xie X, Man D and Huang S 2025 Intelligent prediction and understanding of self-shrinkage in ultra-high performance concrete based on machine learning Case Studies in Construction Materials 22 e04255
[29] Chen X et al 2025 Machine learning-based modelling and analysis of carbonation depth of recycled aggregate concrete Case Studies in Construction Materials 22 e04162
[30] Chaitanya M, Manikandan P, Prem Kumar V, Elavenil S and Vasugi V 2020 Prediction of self-healing characteristics of GGBS admixed concrete using artificial neural network J. Phys.: Conf. Ser. 1716 012019
[31] Aravind N, Nagajothi S and Elavenil S 2021 Machine learning model for predicting the crack detection and pattern recognition of geopolymer concrete beams Constr. Build. Mater. 297 123785
[32] Jagadesh P et al 2024 Examining the influence of recycled aggregates on the fresh and mechanical characteristics of high-strength concrete: a comprehensive review Sustainability 16 9052
[33] Ali T et al 2024 A systematic literature review of AI-based prediction methods for self-compacting, geopolymer, and other eco-friendly concrete types: advancing sustainable concrete Constr. Build. Mater. 440 137370
[34] Taffese W Z, Zhu Y and Chen G 2024 Ensemble-learning model based ultimate moment prediction of reinforced concrete members strengthened by UHPC Eng. Struct. 305 117705
[35] Nagajothi S and Elavenil S 2020 Influence of aluminosilicate for the prediction of mechanical properties of geopolymer concrete—artificial neural network Silicon 12 1011–21
[36] Wu L L, Zou D L and Hao Y F 2024 Exploring the compositional effect of eco-friendly ultra-high performance concrete on dynamic strength based on stacking algorithm and explainable artificial intelligence Developments in the Built Environment 20 100574
[37] Das P and Kashem A 2024 Hybrid machine learning approach to prediction of the compressive and flexural strengths of UHPC and parametric analysis with shapley additive explanations Case Studies in Construction Materials 20 e02723
[38] Miao X, Chen B and Zhao Y 2024 Prediction of compressive strength of glass powder concrete based on artificial intelligence Journal of Building Engineering 91 109377
[39] Zheng X et al 2023 A data-driven approach to predict the compressive strength of alkali-activated materials and correlation of influencing parameters using SHapley Additive exPlanations (SHAP) analysis Journal of Materials Research and Technology 25 4074–93
[40] Marani A and Nehdi M L 2020 Machine learning prediction of compressive strength for phase change materials integrated cementitious composites Constr. Build. Mater. 265 120286
[41] Li Q F and Song Z M 2022 High-performance concrete strength prediction based on ensemble learning Constr. Build. Mater. 324 126694
[42] Sun H, Luo L, Li X and Yuan H 2024 The treated recycled aggregates effects on workability, mechanical properties and microstructure of ultra-high performance concrete Co-reinforced with nano-silica and steel fibers Journal of Building Engineering 86 108804
[43] Oh T, Chun B, Lee S K, Kim G W, Banthia N and Yoo D Y 2024 Effect of high-volume substituted nanosilica on the hydration and mechanical properties of ultra-high-performance concrete (UHPC) Cem. Concr. Res. 175 107379
[44] Awadeen M, Amin M, Bakr R H and Tahwia A M 2024 Mechanical properties, attenuation coefficient, and microstructure of ultra high-performance heavyweight concrete for radiation shielding applications Journal of Building Engineering 82 108395
[45] Esmaeili J, Romouzi V, Kasaei J and Andalibi K 2023 An investigation of durability and the mechanical properties of ultra-high performance concrete (UHPC) modified with economical graphene oxide nano-sheets Journal of Building Engineering 80 107908
[46] Chu H, Gao S, Gao L, An Y and Jiang J 2023 Effects of steel chips on the microstructure, mechanical property, and durability of ultra-high-performance concrete with high elastic modulus Journal of Building Engineering 72 106662
[47] Wang J and Huang Y 2023 Mechanical properties and hydration of ultra-high-performance seawater sea-sand concrete (UHPSSC) with limestone calcined clay cement (LC3) Constr. Build. Mater. 376 130950
[48] Jiang K et al 2023 Mechanical properties of multi-scale mono/hybrid non-metallic fiber-reinforced ultra-high performance seawater sea-sand concrete Constr. Build. Mater. 401 132922
[49] Wu Z, Shi C and Khayat K H 2018 Multi-scale investigation of microstructure, fiber pullout behavior, and mechanical properties of ultra-high performance concrete with nano-CaCO3 particles Cem. Concr. Compos. 86 255–65
[50] Roberti F, Cesari V F, De Matos P R, Pelisser F and Pilar R 2021 High- and ultra-high-performance concrete produced with sulfate-resisting cement and steel microfiber: autogenous shrinkage, fresh-state, mechanical properties and microstructure characterization Constr. Build. Mater. 268 121092